Reducing Peak & Fatigue Mooring Loads: A Validation Study for Elastomeric Moorings

D. Parish [#1], M. Herduin [*2], T. Gordelier [#3], P.R. Thies [#4], L. Johanning [#5]

[#] *Offshore Renewable Energy, College of Engineering, Mathematics and Physical Sciences,*

University of Exeter, Penryn Campus, Penryn, Cornwall, United Kingdom.

[1] d.n.parish@exeter.ac.uk; [3] t.j.gordelier@exeter.ac.uk; [4] p.r.thies@exeter.ac.uk; [5] l.johanning@exeter.ac.uk

[*] *Centre for Offshore Foundation Systems,*

The University of Western Australia, 35 Stirling Highway, Crawley, Western Australia.

[2] manuel.herduin@research.uwa.edu.au

***Abstract*—Fibre ropes are often specified for floating wave and tidal energy device mooring systems. The relatively low axial stiffness goes some way towards mitigation of the peak and fatigue mooring loads. However, the minimum breaking load (MBL) of a fibre rope dictates its axial stiffness and hence the free selection of low axial stiffness is not possible with conventional rope. The resulting mooring stiffness is often sub-optimal, giving rise to elevated peak and fatigue loads. Elastomeric, nonlinear mooring elements solve this by partially de-coupling the axial stiffness from the MBL and offering an initial soft response with increasing stiffness for higher strains. These nonlinear elastomeric moorings have the potential to reduce the peak and fatigue mooring loads as indicated by numerical studies.**

This work uses a validated numerical model to quantify the load reduction achievable by substituting a novel elastomeric tether in place of a conventional fibre rope. Field data is used to validate the base case model of the highly dynamic South West Moorings Test Facility (SWMTF). The base case mooring design utilises Nylon ropes which are subsequently replaced with elastomeric tethers in the validated model.

The results show that the peak mooring loads are reduced substantially upon substituting the elastomeric tethers for the conventional ropes. Subsequently this allows a downward iteration of MBL and axial stiffness towards an optimal condition, providing the lowest achievable load case. In most instances, the optimum iteration outcome also allows a reduction in catenary chain weight.

The reduction in peak tension is accompanied by an increase to the buoy excursion in surge. However, the mean peak excursion increase is 21% whilst the mean peak tension reduction is 66%.

***Keywords*—** Elastomeric mooring, peak load, fatigue, axial stiffness, mooring stiffness, design iteration.

I. Introduction

The mooring system is an important sub-system of any floating marine energy converter (MEC). Deployment of a floating device in highly energetic wave conditions or tidal currents, will inevitably subject the device and the mooring system to correspondingly high magnitude loads. In extreme conditions these loads will be very much greater than those loads experienced ordinarily. These loads, termed extreme loads, drive the engineering design of both the mooring system and the structural elements of the floater. Whilst it is technically feasible to cater for these elevated loads within the mooring design, the cost of components increases in proportion to their rated minimum breaking load (MBL) [1]. This creates a disparity between the cost of the system and the financial returns during operation. Gordelier et al. [2] note that "the capital cost of the mooring system is driven by extreme (peak load) conditions, whilst the revenue is generated under normal operating conditions". It is also important to recognise that the costs relating to the deployment, decommissioning and operation of WEC mooring systems will also contribute to the levelised cost of energy (LCOE) [3] and larger, heavier structural designs will elevate these costs.

Mooring designs for highly dynamic MECs have converged around compliant mooring systems, as recommended by [1], [4] and many others. Mooring lines with low axial stiffness are a key component in the design of compliant mooring systems and fibre ropes are often specified for this reason. However, the axial stiffness of a fibre rope is strongly related to the MBL; designers can find themselves specifying ropes that are stiffer than their preferred solution in order that the tensile strength is adequate to cater for the load case including the factor of safety (FOS).

Elastomeric mooring tethers are being developed to address this conflict between axial stiffness and breaking strength. These tethers partially decouple the two parameters to allow more freedom in the selection of low axial stiffness without compromising the mooring line strength. Designers are then able to select axial stiffness in order that an optimal mooring design achieves the required station keeping whilst minimising the peak and fatigue loads generated in the system. Numerical studies have been conducted to predict the reduction in mooring loads that is possible by using elastomeric tethers [5] and [6]. These studies have indicated that the use of elastomeric mooring tethers can reduce the magnitude of peak loads by as much as 70% [5].

The work presented in this paper follows a staged validation approach:

1. Real data recorded at the SWMTF (section IV.*A*) is used to validate a base numerical model of the SWMTF buoy and mooring system, created with Orcaflex software (sections IV.*B*, IV.*C*). The recorded data includes wave surface elevation, current velocity,

buoy position and mooring loads. This time series data corresponds to a high energy sea state, 9th October 2010, which gives rise to extreme mooring loads.

2. The validated model is then modified to replace the standard Nylon mooring ropes with elastomeric 'Exeter Tethers' of the same MBL (section IV.*D*). Simulations are then performed in three variants: Explicit integration, implicit integration and implicit integration with an alternative interpretation of surface current.
3. The mooring load time series for the elastomeric moorings are analysed and compared against the standard rope configuration (section V).

The elastomeric tether assessed is the Exeter Tether, a patented technology [7] developed by research engineers at the University of Exeter.

II. The Exeter Tether

The Exeter Tether is an assembly comprising a hollow braid polyester rope, a radially compressible core and helically wound textile layers separating these elements and excluding marine growth. The hollow fibre rope is the tensile load carrier and is terminated at each end with an eye splice. The preferred version of the tether utilises seven round strands of EPDM rubber to form the core as shown in Fig. 1. The specific Exeter Tether used in this study, version P1-6, is of this preferred construction, the EPDM having a Shore A hardness of 81. A full description of the Exeter Tether development and proof of concept study is given by [3] with further information on durability by [2].

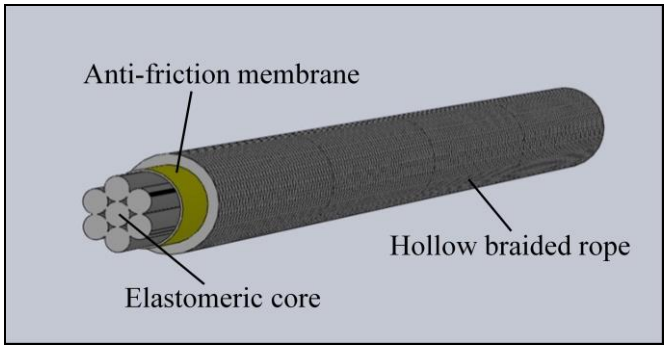

Fig.1 A cutaway illustration of the Exeter Tether construction

A. Exeter Tether Properties

The Exeter Tether exhibits two distinct phases of extension which are discernible by a marked change in axial stiffness. Fig. 2 shows the normalised axial stiffness profile for the P1-6 Exeter Tether in the unworked condition; for comparison, the corresponding axial stiffness of a conventional double braid polyester rope is included [3].

The two phases of axial stiffness are an outcome of the tether's mechanism. Extension of the tether results in the diametric contraction of the hollow braid rope. By resisting radial compression, the elastomeric core controls the extension of the tether. During the first phase of extension the braid angle is high providing the rope strand helices with a large mechanical advantage in compressing the elastomeric core. Simultaneously, the deformation of the seven elastomeric core strands to reduce free space within the core is relatively easy. During the second phase of extension, the free space within the core structure has been minimised and the core is extremely resistant to further compression. Simultaneously, the rope's braid angle is decreased which reduces the mechanical advantage of the rope in compressing the core. Indeed second phase extension relies greatly upon the Poisson's diminution of the core and the extension of the polyester rope strands.

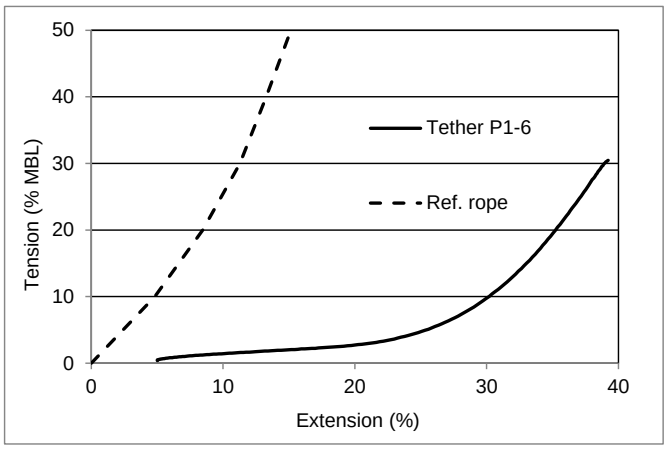

Fig. 2 The normalised axial stiffness for the P1-6 Exeter Tether and a conventional double braid polyester rope

B. General Elastomeric Tether Properties

The two phases of axial stiffness are a common feature of elastomeric tethers. It is necessary that the highly compliant first stage extension reaches a limit so as to finally arrest the excursion of a floating body at a defined extent. In this respect the Exeter Tether is representative of the general performance of elastomeric tethers. Fig. 3 illustrates the axial stiffness profile of the Superflex elastomeric tether and Fig. 4 the Seaflex elastomeric tether; both of these also display two distinct phases of axial stiffness.

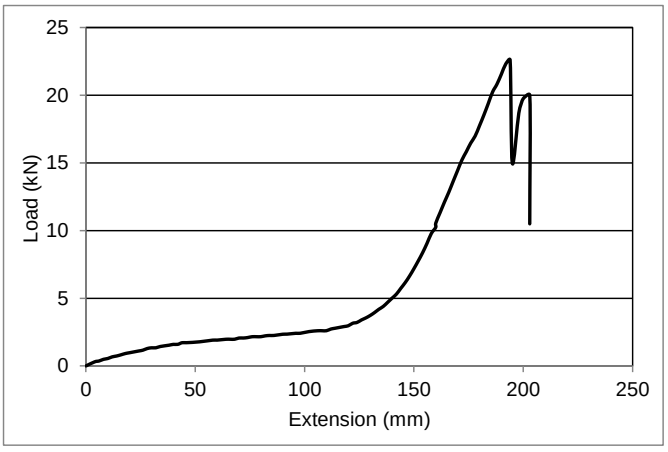

Fig. 3 Axial stiffness profile for the Superflex elastomeric tether during a break test [8].

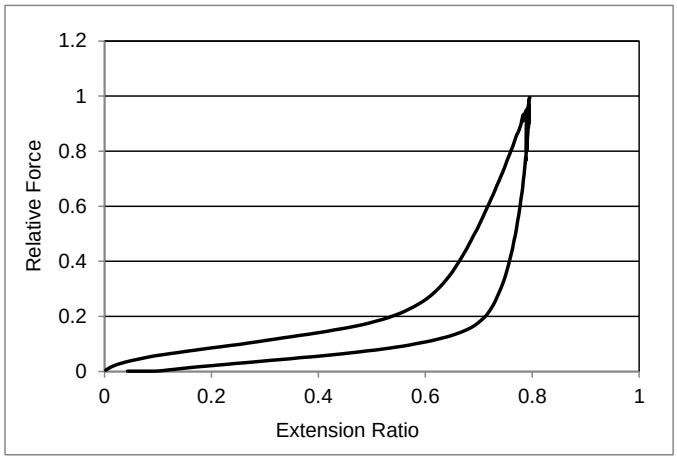

Fig. 4 Axial stiffness profile for the Seaflex elastomeric tether; the full cycle is shown demonstrating the hysteresis of the tether [9].

III. The South West Mooring Test Facility (SWMTF)

The SWMTF is specifically designed as a sea based test platform to advance research in mooring systems and mooring components for highly dynamic floating bodies. It comprises a highly instrumented data buoy, a three limbed catenary mooring system and a seabed mounted acoustic Doppler current profiler (ADCP).

A. SWMTF Buoy

The buoy is constructed around a central steel column assembly. Attached to the central column is a polyurethane foam collar, stainless steel superstructure and galvanised steel ballast. The maximum diameter of the buoy is 2.9 m and the mass properties of the buoy are detailed in Table I.

B. Instrumentation and data

The principal aim of the SWMTF is to effectively monitor and log key operational parameters of a highly dynamic moored, floating device. This data falls broadly into three categories as outlined by [3]:

- Environment – wave, wind, current.
- Dynamics – pitch, roll, yaw, surge, sway, heave, position, heading.
- Mooring loads – vector, axial magnitude.

The seabed mounted ADCP measures and records current and wave data, which is downloaded upon ADCP retrieval.
The remaining data is collated by an on-board SCADA system, located within a sealed acetal polymer unit which sits within the central framework of the buoy superstructure. Data is routinely transmitted in 10 minute zip files to a local shore station via a dedicated Wi-Fi bridge. It can also be retrieved manually via Wi-Fi access with a laptop within 200 m of the buoy, or using a hard wire directly connected into the SCADA unit. A summary of the main SWMTF instrumentation is provided in Table II.

TABLE I
Mass Properties of the SWMTF Buoy

Mass property	Value	Unit
Weight in air	3243	kg
Centre of gravity (below mean sea level)	499	mm
Moment of inertia (pitch/roll)	4250	$kg.m^2$
Moment of inertia (yaw)	1179	$kg.m^2$

TABLE II
Primary SWMTF Instrumentation

Data	Frequency (Hz)	Sensor	Location
Wave conditions	2	RDI Workhorse Sentinel ADCP	Sea bed
Water current	2	RDI Workhorse Sentinel ADCP	Sea bed
Wind conditions	4	Gill Windsonic anemometer	Buoy structure
Kinematics	20	MotionPak, 6-axis inertial sensor	SCADA module
Position	10	Trimble DGPS rover station	SCADA module
Heading	20	Tilt compensated flux-gate compass	SCADA module
Mooring load vectors	20	Bespoke tri-axial load cells (69 kN)	Underside of buoy
Axial mooring load	20	Bespoke axial load cells (69 kN)	Top end mooring

C. Mooring system

The SWMTF mooring system comprises three catenary mooring limbs, each designed for a peak load case of 207 kN including a factor of safety of 3. The standard mooring limb composition from the buoy to the seabed is: 20 m x 44 mm nylon rope; 36 m x 24 mm open link chain; 5 m x 32 mm studlink chain; 1.1 tonne drag embedment anchor. These individual line components are connected using appropriate safety shackles with axial swivels also incorporated at three positions to prevent torsion in the limb. The orientation of the SWMTF mooring system is detailed in Fig 5.

The water depth at the SWMTF site is 28 m relative to chart datum and the tidal range peaks at 5.9 m. The seabed is predominantly of fine sand with some loose stone deposits.

D. SWMTF location

The SWMTF is located in Falmouth Bay off the south coast of Cornwall, UK. The site is in the lee of the Lizard peninsula for the prevailing sea conditions but is exposed to waves emanating from the east and south east; waves from the east having a fetch of approximately 400 km.

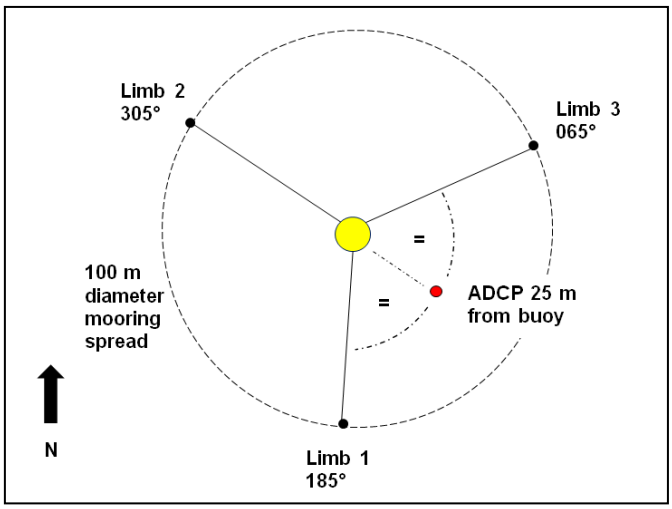

Fig. 5 Plan view of the SWMTF mooring spread and ADCP position

IV. Methodology

The methodology employed in this work is as follows:

- Measured data from the SWMTF is examined in order that a suitable peak energy event is identified.
- A numerical model of the SWMTF is configured; the environmental conditions are set according to the measured data.
- Validation of the base model is conducted by comparing the simulation outputs with the measured data.
- Mechanical properties of the P1-6 Exeter Tether are substituted for those of the Nylon ropes in the model; equivalence of breaking strength is maintained at the initial stage.
- Simulations are performed in an iterative manner; a reduction to the peak limb tension provides feedback to the model via reduced tether strength and correspondingly lower axial stiffness (Fig 2).
- Reduced catenary chain mass is also included in the iteration of mooring stiffness by means of reduced diameter chain section.
- Orcaflex software is used to assess the mooring system stiffness for each case of the iteration simulations; the relationship between system stiffness and peak load is examined.

A. Measured Data From the SWMTF

An analysis is conducted of the environmental conditions leading to a peak mooring load event, as measured by the axial load cells. The deployment period from September 2010 – September 2011 was reviewed and four peak events were identified, with peak mooring loads ranging from 50-55 kN. Three of the four events occurred on Mooring Limb 3, which is the predominant load bearer in easterly sea conditions. The peak event, leading to a 55 kN peak load on Mooring Limb 3, and occurring at 09:32 on 9th October 2010, was selected for further analysis as detailed in the following sections.

1) Wave Data: Wave data is analysed using Teledyne WavesMon software, evaluating data in 17.07 minute bursts; the time period selected for the analysis is 09:18 – 09:35. The directional spectrum for this period is detailed in Fig. 6 and demonstrates a distinctly unimodal sea dominated by waves emanating from the east. The non-directional wave parameters over the same time period are detailed in Table III.

TABLE III
NON-DIRECTIONAL WAVE PARAMETERS FOR PEAK WAVE EVENT 09:18 – 09:35, 09/10/2010.

Parameter	Value
H_s (significant wave height)	2.51 m
T_p (peak wave period)	6.70 s
H_{max} (maximum wave height)	4.4 m

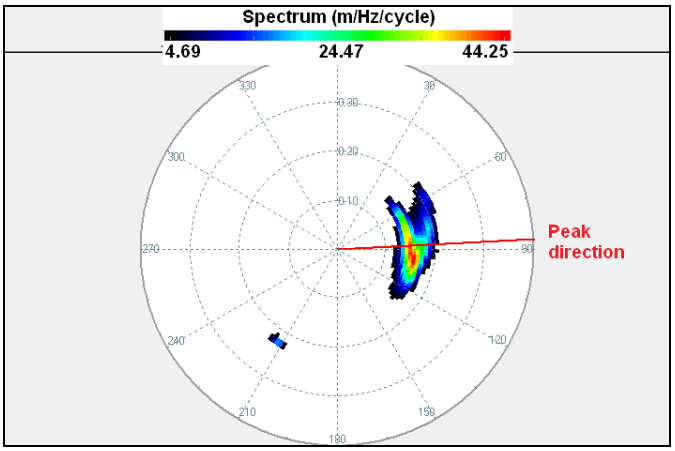

Fig. 6 Directional spectrum for peak wave event at SWMTF 09:18 – 09:35, 09/10/2010

A 240 second duration subset of the wave burst data is identified. This subset of data corresponds to one wave set, a group of high energy waves, which accounts for the peak mooring load under examination. The subset of data includes the relative lull in wave activity at either end of the wave set. The wave surface elevation during this 240 second period is shown in Fig 7.

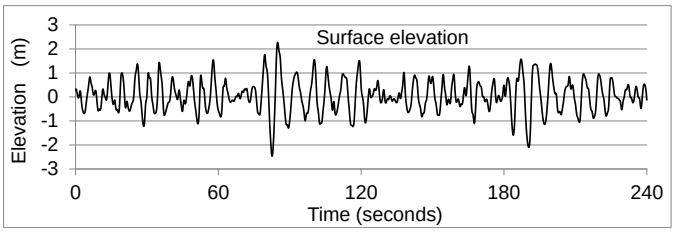

Fig. 7 Wave surface elevation for the 240 second data subset

2) Mooring Line Tension: Mooring limb 3 axial tension data relating to the identified 240 second time period is detailed in Fig. 8. The 55 kN peak load event occurs at T = 188 seconds coinciding closely to the second of two peak waves shown in Fig. 7.

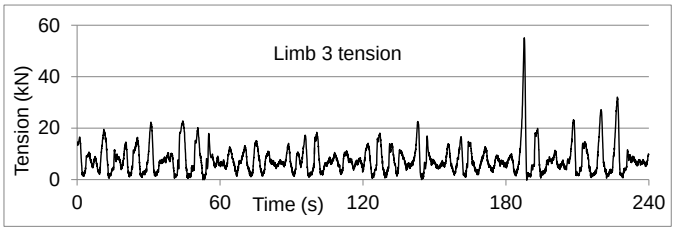

Fig. 8 Mooring tension in limb 3 for the 240 second data subset

3) Buoy Position Data: A peak buoy excursion of approximately 6 m occurs at T = 188 seconds, aligning with the peak tension. The data for buoy excursion during the 240 second period is given as Fig. 9.

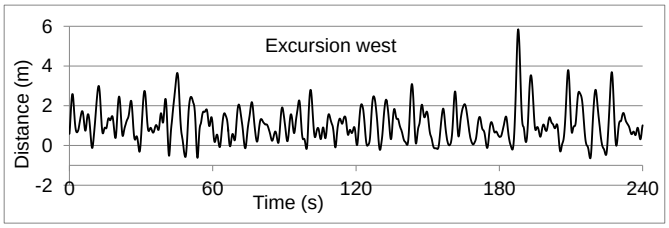

Fig. 9 Buoy excursion to the west for the 240 second data subset

4) Wind Data: Wind parameters corresponding to the 240 second period are detailed in Table IV.

TABLE IV
WIND PARAMETERS MEASURED DURING THE 240 SECOND PERIOD

Parameter	Value
Mean wind speed	2.51 m/s
Maximum wind speed	6.70 m/s
Minimum wind speed	4.4 m/s
Mean direction (emanating from)	089°

5) Current Data: The current profiles provided by the ADCP are shown for eastward flow in Fig.10 and northward flow in Fig 11. This current data provided by a seabed mounted ADCP presents some uncertainty for the upper profile bins. The water depth is changing with the wave activity leading to intermittent null returns. The approach taken here is to simplify this flow and represent it as two alternative vector interpretations at the surface. The two vectors are given in Table V together with their assumed eastward and northward components, these components being represented by dashed grid lines on Figs. 10 and 11. A power law decay of velocity with depth is assumed, having an exponent of 7.

TABLE V
SURFACE CURRENTS DURING THE 240 SECOND PERIOD

Vector	Eastward component	Northward component	Resolved Speed	Heading
1	50 mm/s	-500 m/s	0.50 m/s	174°
2	-320 mm/s	-550 mm/s	0.64 m/s	210°

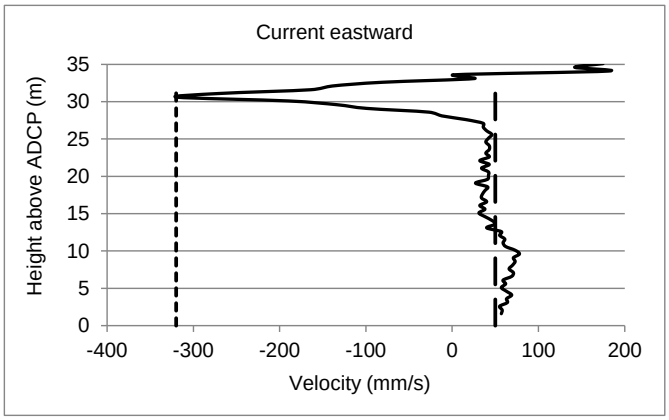

Fig. 10 Eastward current profile with assumed eastward components indicated for simplified interpretations 1 (RH) & 2 (LH).

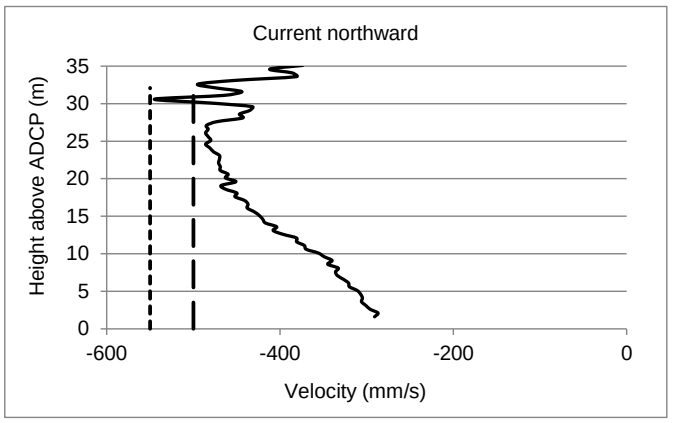

Fig. 11 Northward current profile with assumed northward components indicated for simplified interpretations 1 (RH) & 2 (LH).

B. Numerical Model

1) General Details: The numerical models and simulations are conducted using OrcaFlex™ (version 9.8a). This commercial software is a time-domain finite element solver that computes the coupled response of a floating structure and its mooring system. Mooring lines are represented with a discretised model which is a series of visco-elastic segments with mass components on both extremities of segments. The Morison's equation is applied to compute the forces on each segment of the mooring line and on the wet surfaces of the floating structure. Wind loading is modelled as a static force acting on fictitious planes.

2) Model Construction: The buoy is modelled as a 6D spar buoy with mass properties as given in Table I. The surfaces of the buoy are represented by five cylinders as listed in Table VI. A comparison of the wireframe model and the general assembly drawing of the buoy is provided in Fig. 12. Hydrodynamic properties are assigned to the modelled buoy according to Table VII. The Line Wizard within Orcaflex is used to assign mass, mechanical and hydrodynamic properties to the mooring lines; the axial stiffness profile for the Nylon ropes is referenced from sales material [10].

TABLE VI
MODELLED BUOY DIMENSIONS

Cylinder no.	Length (m)	Diameter (m)
1 (upper)	0.940	2.900
2	0.230	2.175
3	0.230	1.450
4	0.490	0.360
5 (lower)	0.210	1.100

TABLE VII
MODELLED BUOY HYDRODYNAMIC PROPERTIES

Property	Condition	Formula	Coefficient
Drag forces	normal area (m^2)	Ø x L	1.0
	axial area (m^2)	(π x $Ø^2$) / 4	1.0
Drag moments	normal area moments (m^5)	(L x $Ø^4$) / 32	1.0
	axial area moments (m^5)	$Ø^5$ / 60	1.0
Added mass	normal	-	(Ca) 1.0
	axial	-	(Ca) 0.64
Inertia	normal	-	(Cm) 2.0
	axial	-	(Cm) 1.64

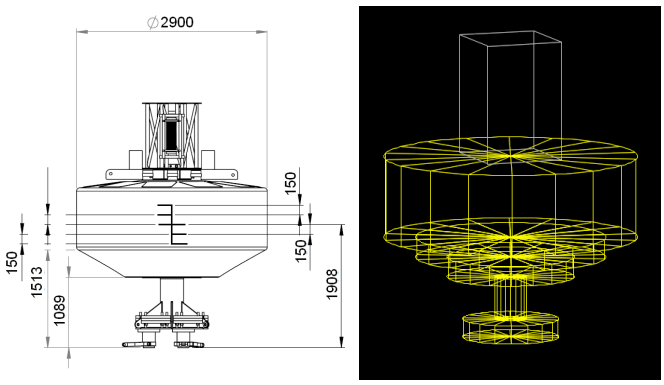

Fig. 12 The general assembly drawing of the SWMTF buoy (LH) and the wireframe Orcaflex model (RH) shown for comparison.

C. Validation of the Numerical Model

Validation of the base case model, with nylon mooring ropes, is conducted according to two separate methods to provide rigour:

1) Time History Wave Data: The wave condition is input as a 1200 second time series of surface elevation which encompasses the 240 second period of interest. The Orcaflex software performs a fast Fourier transform (FFT) on the full 1200 second data set. The programme then assigns a single Airy wave to each of the frequency components that result from the transform and these are used in combination to recreate the waveform described by the input data [11]. This method accurately reproduces the surface elevation time series within the simulation but is computationally demanding and correspondingly slow to process.

Firstly a simulation is performed using the explicit integration method; the magnitude and timing of the simulated peak mooring load is compared to the real data. Fig. 13 shows the simulated tension for limb 3 of the mooring system together with the real data for comparison. The peak load of 48 kN occurs at T = 187 s; this agrees well with the real peak of 55 kN occurring at T = 188 s. Secondly, the simulation is repeated using implicit integration rather than explicit. Lastly, a further implicit integration is conducted, this time using the alternative current interpretation accounting for wind and wave effects (see Table V). These implicitly solved simulations returned peak tensions of 43 kN at T = 194 s and 48 kN at T = 86 s respectively, showing less alignment with the timing of the real data than the explicit simulation. Orcina describe the explicit integration method as robust and reliable but requiring much more computation time than the implicit integration. They describe the implicit integration as much quicker but warn that the accuracy can be sensitive to the time step selected for use [11].

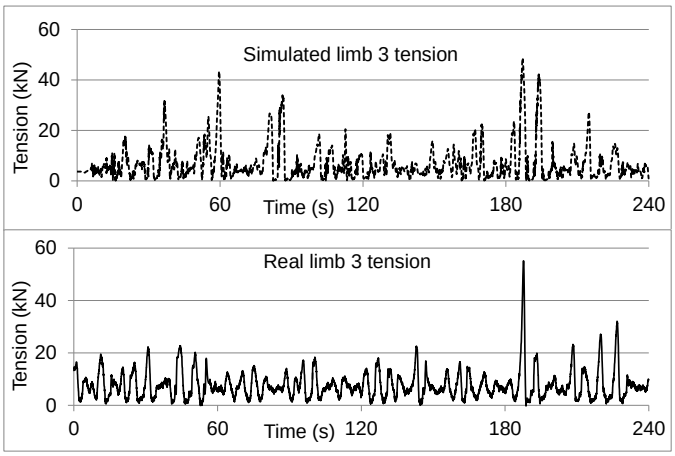

Fig. 13 Explicit simulation outcome for mooring tension in limb 3 (upper) and real limb 3 tension data shown for ease of comparison (lower).

2) JONSWAP Spectrum Wave Parameters: Environmental conditions recorded by the ADCP for three alternative peak load events are input to the model (Table VIII, simulations A, B&C). Wave conditions are specified by inputting the appropriate JONSWAP spectrum parameters. This method is far less computationally demanding but does not reproduce the recorded surface elevation time series. Simulations are performed using the implicit integration method; the magnitude of the simulated peak load is compared to the real data. Table VIII summarises the conditions and the comparison of real and simulated mooring tension.

TABLE VIII
ADDITIONAL SIMULATION CONDITIONS AND COMPARISON

Parameter	Simulation A	Simulation B	Simulation C
Wave height (Hs)	2.47 m	2.39 m	2.62 m
Period (Tp)	5.90 s	6.90 s	7.70 s
Mean depth	28.5 m	31.0 m	31.9 m
Wave direction	122°	177°	172°
Current direction	196°	225°	030°
Current velocity	0.30 m/s	0.15 m/s	0.15 m/s
Comparison			
Peak load: real data	37 kN	20 kN	60 kN
Peak load: simulation	30 kN	23 kN	60 kN

D. Exeter Tether Performance Simulations

The simulation method utilising time history wave data is selected for the tether performance simulations (as detailed in section C, method 1). The peak loads are event related and this method reproduces the causal events most accurately. Three series of iterated simulations are performed as follows:

- Explicit integration method
- Implicit integration method
- Implicit integration method using the alternative surface current detailed in Table V.

Different simulation series are used so that any alignment of results improves confidence in the outcomes. In each iteration series the starting condition is the substitution of the Exeter Tether for the nylon ropes in the model; the MBL of the tether is set to be equivalent to the nylon rope which in turn defines the axial stiffness according to Fig. 2. Mass properties and hydrodynamics geometry are set to the MBL according to predicted scaling of the tether shown in Fig.14. The tether scaling is based upon maintaining geometric proportions of the cross section which governs the increase of MBL. A full description of Exeter Tether scaling is given in [3].

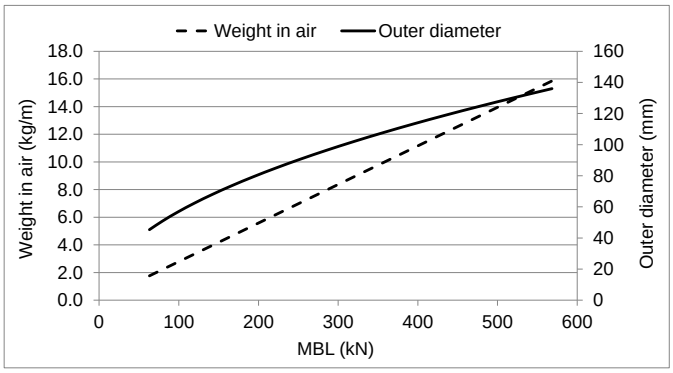

Fig. 14 Scaling of the Exeter Tether properties, weight and diameter with MBL.

For each of the three series, the iteration is progressed according to the following:

- The peak load result from a simulation is fed into the next simulation in the form of reduced axial stiffness, weight and diameter of the tether according to Fig. 2 and Fig. 14. The FOS 3 is maintained.
- When the reduction in peak load allows, the catenary chain bar diameter is reduced from 24 mm to 19 mm and then again to 16 mm whilst maintaining a FOS = 3, this is done using the Orcaflex Line Wizard.
- If reducing the chain diameter causes an increased peak load, the original chain diameter is restored and iteration is continued with the tether properties only.
- Iterations continue until the optimal condition, providing minimum peak tension has been established.

E. Mooring System Stiffness

Orcaflex software is further utilised to conduct a quasi-static analysis of the mooring system stiffness for each of the mooring configurations from the iteration simulations. Analysing the whole system stiffness under horizontal floater displacement follows the methodology utilised by [12] and [13].

The existing models from the iteration series are modified to remove the wave, wind and current forces. These are replaced by an 'applied global load' acting on the SWMTF buoy. The load acts horizontally in a direction that is directly away from anchor no. 3. The applied horizontal load ramps up slowly from zero to 50 kN linearly over 500 seconds; the displacement velocity of the buoy is low enough to disregard drag effects. An implicit simulation is performed concurrently with the applied load.

Results are taken for tension at the top of limb 3 and the buoy displacement. For each of the 15 quasi-static simulations, the tangent modulus for mooring system stiffness is determined at the tension value corresponding to that mooring configuration's dynamic simulation peak tension result.

V. RESULTS

The Peak tension outcomes of the 15 simulations that comprise the three iteration series are illustrated in Fig. 15. The iteration steps are detailed in Table IX together with the peak tension outcomes. The optimal condition for each iteration series is highlighted in bold for clarity.

The reductions to peak mooring tensions are summarised for all three iteration series in Table X. Results for the buoy excursions are included together with the excursion results for the base case simulations. The mean result from the three series is a 66% reduction to the peak mooring load with a 21% increase to the excursion. The results of the quasi-static mooring stiffness analysis are summarised in Fig.16. The plot of the peak limb tensions (Table IX) against the coincident mooring system stiffness approximates to a linear trend with a least squares regression giving $R^2 = 0.94$.

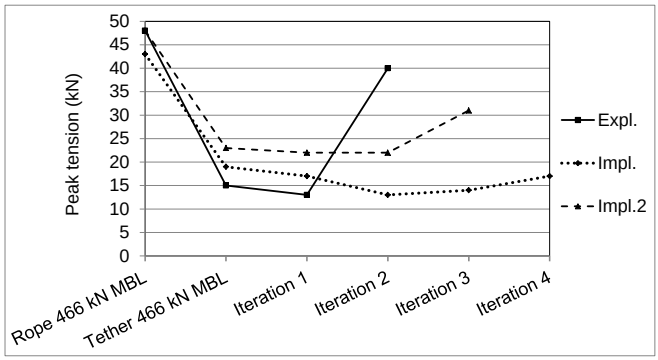

Fig. 15 Peak tension outcomes from the 15 simulations

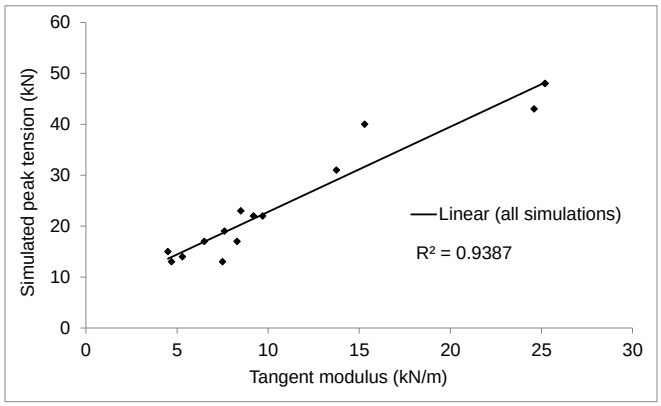

Fig. 16 Mooring system tangent modulus vs simulated dynamic peak tension (all simulations)

TABLE IX
DETAILS OF THE ITERATION STEPS

Iteration	Explicit	Implicit	Implicit 2
Nylon Rope	466 kN MBL	466 kN MBL	466 kN MBL
	24 mm chain	24 mm chain	24 mm chain
	48 kN peak	43 kN peak	48 kN peak
Exeter Tether	466 kN MBL	466 kN MBL	466 kN MBL
	24 mm chain	24 mm chain	24 mm chain
	15 kN peak	19 kN peak	23 kN peak
1	**146 kN MBL**	206 kN MBL	**466 kN MBL**
	24 mm chain	24 mm chain	**19 mm chain**
	13 kN peak	17 kN peak	**22 kN peak**
2	146 kN MBL	**206 kN MBL**	**223 kN MBL**
	19 mm chain	**19 mm chain**	**19 mm chain**
	40 kN peak	**13 kN peak**	**22 kN peak**
3	-	152 kN MBL	223 kN MBL
	-	19 mm chain	16 mm chain
	-	14 kN peak	31 kN peak
4	-	152 kN MBL	-
	-	16 mm chain	-
	-	17 kN peak	-

TABLE X
SUMMARY OF PEAK TENSION AND EXCURSION OUTCOMES

Parameter	Explicit	Implicit	Implicit 2
Base case peak tension	48 kN	43 kN	48 kN
Optimal peak tension	13 kN	13 kN	22 kN
Load reduction	73%	70%	54%
Base case excursion	10.1 m	8.3 m	8.2 m
Revised excursion	10.8 m	10.2 m	10.8 m
Excursion increase	7%	23%	32%

VI. DISCUSSION

The validation of the base case Orcaflex model with real data is an important stage of this work. Explicit integration simulation is the more reliable option but increases the computational load of the simulation. In addition to this, a further significant computational load is added when using the time history wave data functionality. To alleviate this slightly, the current flow which has some uncertainty associated with it is simplified. To optimise the confidence in the outcomes whilst minimising the simulation processing time, three different formats of simulation are adopted using time history wave data and a forth format is employed using a specified wave spectrum. The explicit integration simulation with time history wave data provided close agreement with the real data in terms of peak tension magnitude and timing.

The Exeter Tether performance simulations also employ three variants of simulation format. This reflects the understanding that the models and simulations are approximations; by varying the technique within sensible bounds, a greater confidence can be achieved in the collective outcome. Referring to Fig. 15, it might be assumed from the Orcina advice that the explicit series is the most accurate but it is useful to have the trend corroborated by the other two series.

This work confirms that elastomeric mooring tethers have the capacity to significantly reduce peak mooring loads; in this study the peak load was reduced by a mean factor of three in consideration of all three series. The work also suggests that each mooring system has an optimal stiffness which will minimise the peak loading for a given maximum excursion. The ‘convex’ curves in Fig. 15 show that too much compliance will increase peak loading in the same way that too much stiffness will.

The quasi-static analysis helps by supporting an intuitive assumption: If the floater’s excursion is finally limited by a stiff restraint, the peak load will be higher than if arrested by a soft restraint. Interpreting this in relation to the two stages of axial stiffness shown in Figs. 2, 3 and 4, the optimal elastomeric tether for a given system and maximum allowable excursion might be designed such that:

- The full extent of stage one extension is sufficient that it just allows stage two to initiate before the maximum excursion is realised.

- The axial stiffness of stage one is just sufficient to absorb the majority of the peak excursion energy before stage two initiates.

An analogy may help to illustrate this: Consider a train coming to halt at a terminus platform. If too much braking is applied, the train will come to halt earlier than necessary and the braking force will be higher than necessary. Conversely, if the braking is insufficient the train will have too much energy when it is arrested by the buffers. In this analogy, the braking represents the first stage of extension and the buffers, the second.

In addition to observing peak mooring loads, it is important to consider the fatigue load case. Highly cyclic, high magnitude loads will eventually cause component fatigue failures. A reduction in magnitude and frequency of high load events will reduce the fatigue damage to the individual mooring components; fatigue damage is primarily driven by peak load events as shown in [14]. A detailed quantification of fatigue loads for the different mooring configurations incorporating the tether is subject to ongoing work.

VII. CONCLUSION

This work has utilised a validated numerical model of the SWMTF to evaluate the performance of an elastomeric mooring tether. The use of real data from the SWMTF to validate a base case numerical model significantly reduces the inherent uncertainty associated with such numerical techniques. By adopting a spread of simulation formats and achieving good alignment of results, the remaining uncertainty with the modelling and simulation process is reduced. Previous outcomes of non-validated numerical modelling that suggest peak load reductions of 70% are supported by this work.

Further research work based on field load data and the physical field demonstration of the tether is also in progress. The EU project Open Sea Operating Experience to Reduce Wave Energy Cost (OPERA) [15] will deploy a version of the described elastomeric mooring system. A measured assessment of the peak mooring load reduction will be made for the Oceantec wave energy converter under operating and extreme conditions at the Basque Bimep test site.

ACKNOWLEDGMENTS

This work was partly funded by the EPSRC (UK) grant for the SuperGen United Kingdom Centre for Marine Energy Research (UKCMER) [grant number: EP/P008682/1]. The development of the Exeter Tether was partly funded by the Open Innovation Platform, supported by the Higher Education Council for England. The authors would also like to acknowledge the support from Lankhorst Ropes throughout the technology development.

REFERENCES

[1] R. E. Harris, L. Johanning, and J. Wolfram, “Mooring systems for wave energy converters : A review of design issues and choices,” *3rd Int. Conf. Mar. Renew. Energy*, pp. 1–10, 2004.

[2] T. Gordelier, D. Parish, P. Thies, and L. Johanning, “A Novel Mooring Tether for Highly-Dynamic Offshore Applications; Mitigating Peak and Fatigue Loads via Selectable Axial Stiffness,” *J. Mar. Sci. Eng.*, vol. 3, no. 4, pp. 1287–1310, 2015.

[3] D. Parish, “A novel mooring tether for highly dynamic offshore applications,” PhD thesis, 2015.

[4] L. Johanning, G. H. Smith, and J. Wolfram, “Measurements of static and dynamic mooring line damping and their importance for floating WEC devices,” *Ocean Eng.*, vol. 34, no. 14–15, pp. 1918–1934, 2007.

[5] P. Mc Evoy, “Combined Elastomeric & Thermoplastic Mooring Tethers,” *4th Int. Conf. Ocean Energy, Dublin, Ireland. 2012.*

[6] P. R. Thies, L. Johanning, and P. McEvoy, “A novel mooring tether for peak load mitigation: Initial performance and service simulation testing,” *Int. J. Mar. Energy*, vol. 7, pp. 43–56, 2014.

[7] D. N. Parish and L. Johanning, “Mooring limb,” US 8807060 B2, 2014.

[8] Supflex, “Superflex mooring test result,” [online], Available: http://supflex.com/home4.html

[9] P. Casaubieilh, F. Thiebaut, W. Sheng, C. Retzler, M. Shaw, and Y. Letertre, “Performance improvements of mooring systems for wave energy converters,” *Renew. Energies Offshore – Guedes Soares ©*, no. Wang 2013, pp. 897–903, 2015.

[10] Bridon, “Fibre rope catalogue,” *Edition 3*, p. 32, 2011.

[11] Orcina, "Orcaflex Manual", *Version 9.4a.*

[12] A. Pecher, A. Foglia, and J. Kofoed, “Comparison and Sensitivity Investigations of a CALM and SALM Type Mooring System for Wave Energy Converters,” *J. Mar. Sci. Eng.*, vol. 2, pp. 93–122, 2014.

[13] J. Fitzgerald and L. Bergdahl, “Considering Mooring Cables for Offshore Wave Energy Converters,” *Proc. 7th Eur. Wave tidal Energy Conf.*, 2007.

[14] P. R. Thies, L. Johanning, V. Harnois, H. C. M. Smith, and D. N. Parish, “Mooring line fatigue damage evaluation for floating marine energy converters: Field measurements and prediction,” *Renew. Energy*, vol. 63, pp. 133–144, 2014.

[15] Open Sea Operating Experience to Reduce Wave Energy Cost. uropean Union’s Horizon 2020 research and innovation programme under grant agreement No 654.444. http://opera-h2020.eu/